

A Study on the Electrodeposited Cu-Zn Alloy Thin Films



RASIM ÖZDEMİR, İSMAIL HAKKI KARAHAN, and ORHAN KARABULUT

In this article, electrochemical deposition of the nanocrystalline $\text{Cu}_{1-x}\text{Zn}_x$ alloys on to aluminum substrates from a non-cyanide citrate electrolyte at 52.5, 105, 157.5, and 210 A m^{-2} current densities were described. The bath solution of the $\text{Cu}_{1-x}\text{Zn}_x$ alloys consisted of 0.08 mol L^{-1} $\text{CuSO}_4 \cdot 5\text{H}_2\text{O}$, 0.2 mol L^{-1} $\text{ZnSO}_4 \cdot 7\text{H}_2\text{O}$, and 0.5 mol L^{-1} $\text{Na}_3\text{C}_6\text{H}_5\text{O}_7$. The effect of the current density on the microstrain, grain size, phase structure, and DC electrical resistivity behavior was investigated. The electrolyte was investigated electrochemically by cyclic voltammetry (CV) studies. A scanning electron microscope (SEM) was used to study the morphologies of the deposits. Deposited alloys were investigated by energy-dispersive X-ray spectroscopy (EDX), X-ray diffraction (XRD), and four-point probe electrical resistivity techniques. With an increase in applied current density values from 52.5 to 210 A m^{-2} , the amount of deposited copper in the alloy was decreased significantly from 65.5 to 16.6 pct and zinc increased from 34.4 to 83.4 pct. An increase in the current density was accompanied by an increase in grain size values from 65 to 95 nm. SEM observations indicated that the morphology of the film surface was modified to bigger grained nanostructures by increasing the current density. The XRD analysis showed alloys have a body-centered cubic (bcc) crystal structure with preferential planes of (110) and (211). Furthermore, four-point measurements of the films revealed that the resistivity of the deposited films was tailored by varying current densities in the electrolyte.

DOI: 10.1007/s11661-016-3715-0

© The Minerals, Metals & Materials Society and ASM International 2016

I. INTRODUCTION

THERE are many technological processes to fabricate metallic alloy thin films. Electrodeposition is the most commonly used one due to technical and environmental advantages. The electrochemical deposition method has some considerable benefits such as low-cost, convenience and allows for controlling of multiple experimental parameters. Improved performance of the electrodeposited alloys mainly depends on the controlled deposition parameters. The mechanism of the growth and nucleation of the alloys as well as their homogeneity in the metal matrix can be modified by many parameters such as electrolyte composition, electrode design, pH, the electrolyte type, applied potential, deposition temperature, type of the counter electrode, and the applied current density.^[1] Area of the anodic current density can be controlled by adjusting geometry and location of the anode (electrode).^[2]

Being an interesting material, Cu-Zn alloys have widely been studied as a coating material over the last two decades due to superior properties. Consisting of a

great number of features of the Zn alloys, especially Cu-Zn alloys, are very attractive materials for industrial applications, such as corrosion protection of steel, adhesion to steel, decorative values, and as electrodes for batteries.^[3]

Old commercial electrodeposition methods for deposition of the Cu-Zn thin film alloys in cyanide-based electrolytes produces useful coatings, but usage and disposal of the cyanide is not practical and environmental pollutions emerge.^[4] Hence, a great effort has been made in research of the reasonable alternative electrolytes.^[4-16] These non-cyanide baths have been resulted fabrication of the satisfactory depositions. Because of the low reproducibility, poor adhesion, and unusual colorations problems, non-cyanide baths have not been accepted in a commercial manner. Some researchers designed a cyanide-free alkaline Cu-Zn electrolyte with sorbitol as the complexing agent.^[4] Most of these reports have revolved around electrolytic solutions of glycerol,^[5-7] sorbitol,^[7] glucoheptonate,^[8] pyrophosphate,^[9,10] citrate-based cysteine and benzotriazole,^[11] tartrate,^[12,13] ionic-liquid choline acetate,^[14] trilonate,^[15] D-mannitol,^[7,16] glycine,^[17,18] gluconate-sulfate,^[19] and citrate.^[20-24] Among them, citrate baths were used in the electrodeposition of the Cu,^[25] Zn,^[26] and Cu-Zn alloys^[27,28] because ligands of the citrate ions have low molecular mass.^[29] It is possible to deposit excellent Cu-Zn alloy coatings from citrate-based electrolytes.^[11] Several papers reported that optimization of the plating conditions for Cu-Zn alloys depends on the

RASIM ÖZDEMİR, Assistant Professor, is with the Kilis Vocational High School, 7 Aralık University, Kilis 79000, Turkey. İSMAIL HAKKI KARAHAN, Professor, is with the Department of Physics, Mustafa Kemal University, Hatay 31000, Turkey. Contact e-mail: ihkarahan@gmail.com ORHAN KARABULUT, Professor, is with the Department of Physics, Pamukkale University, Denizli 22000, Turkey.

Manuscript submitted May 8, 2015.

Article published online September 6, 2016

nature and type of particle to be co-deposited, particle size, zeta potential, bath type, *etc* [4,11,28–33]

This article reports the effect of current density on the elemental content, microstructure, electrochemical properties, electrical resistivity, morphology, and phases of the deposited alloys as a plating parameter. The study is based on using a simple aqueous acidic sulfate solution as the plating bath. The acidic plating bath is easy to prepare and control, and it allows for investigating the effect of various coating parameters. In the process control, the information about the grain size of materials is very important. This method may be useful to predict and/or control multiple deposit properties like visual appearance, deposit stress, electrical properties, *etc*. To develop an understanding of the role of the applied current density, as an electrodeposition parameter, the coating structure is investigated.

II. EXPERIMENTAL DETAILS

$\text{Cu}_{1-x}\text{Zn}_x$ alloys were deposited on aluminum substrates from citrate and non-cyanide citrate baths at various current densities. Electrodeposition of the Cu-Zn alloy thin films was performed at four different current densities of 52.5, 105, 157.5, and 210 A m^{-2} in a traditional glassy cell (nonstirred) to investigate the effects of current intensity. The pH of all bath solutions was adjusted to 5.8. Experimental deposition parameters and bath compositions of the Cu-Zn alloys are shown in Table I.

All plating baths were prepared from high-purity chemicals and double-purified water. Commercially provided aluminum plates were used as substrates. The reference electrode was a saturated calomel electrode (SCE), and the counterelectrode was a platinum wire. Prior to the deposition, the aluminum substrates were glossed, degreased, and activated by dipping in a 1-mol L^{-1} NaOH surfactant at 343 K (70 °C) during 5 minutes and finally rinsed to the double-purified water (18 $\text{M}\Omega$ cm) and dehydrated with fresh air. The pH values were adjusted with sodium hydroxide or sulfuric acid (Hanna Scientific pH-meter). The coatings were deposited on aluminum substrates, which were subsequently stripped from the films by using 10 pct NaOH solution. The reason for selection of the aluminum substrates was to remove Cu-Zn films easily from substrates for the electrical resistivity measurements to eliminate the effect of substrate resistivity. Thickness of the films was approximately 1 μm . Cyclic voltammetry experiments

were performed at 10 mV s^{-1} by scanning initially positive toward negative potentials. The applied potentials were recorded from +0.5 V *vs* SCE (beginning voltage) to -1.6 V and then completed at +0.5 V *vs* SCE to show the reaction of the substrate under the positive and negative polarizations.

The crystallographic structure of the Cu-Zn alloys was analyzed with a Rigaku diffractometer.^[34] The X-ray diffractometer (XRD) was performed at 30 mA and 30 kV, with a 2θ range of 20 to 90 deg using $\text{CuK}\alpha$ radiation at a rate of 0.05 deg, $2\theta/0.5$ seconds.

The surface morphology of the samples was observed using a scanning electron microscope (SEM, JEOL JSM-5500LV, Japan) under 10,000 times magnification. XRD measurements and EDX analysis were performed to the thin films deposited at 52.5, 105, 157.5, and 210 A m^{-2} current densities.

Electrical resistivity experiments for the thin films deposited at 52.5, 105, 157.5, and 210 A m^{-2} were performed with the four-point technique^[35] using a Keithley 2400 current-voltage source at a temperature range of 100 K to 400 K (-173 °C to 127 °C). Experiments were performed using two methods: a Janis liquid nitrogen-cooled and a closed-cycle helium refrigerator. The temperatures of the thin films were accurately monitored and controlled with a Lake Shore 331 temperature controller. Thin films were cut in the form of squares for measurements. Electrical contacts were performed using a silver paint.

III. RESULTS AND DISCUSSION

A. $\text{Cu}_{1-x}\text{Zn}_x$ Platings

Cyclic voltammetry studies were performed for characterization of the Cu-Zn electrolyte. Figure 1 shows the voltammetric responses of aqueous solutions at pH 5.8 and temperature of 293 K (20 °C) containing Cu, Zn ions with trisodium citrate on the aluminum substrate. As shown in Figure 1, the anodic part in the cyclic voltammogram comprise one anodic current peak for thin film. This also shows that the thin film dissolution occurs under 1-V value. In general, the anodic process shows an anodic dissolution peak at 101 mV *vs* SCE. To deposit an alloy composed of Cu and Zn, the electrode must be set at a potential value where both copper and zinc are reduced.

The current density is fully stable between -0.4 and -1.2 V *vs* SCE. This stability is a sign of the successfully aerated plating bath. No current was observed until the

Table I. Electrolyte Composition and Deposition Conditions of the Cu-Zn Alloys Electrodeposited on Aluminum Substrate at pH 5.8 and 293.15 K (20 °C) Different Current Densities for One Hour

Sample	Electrolyte Composition (mol L^{-1})			Current Density (A m^{-2})	Aluminum Substrate (cm^2)
	$\text{CuSO}_4 \cdot 5\text{H}_2\text{O}$	$\text{ZnSO}_4 \cdot 7\text{H}_2\text{O}$	$\text{Na}_3\text{C}_6\text{H}_5\text{O}_7$		
$\text{Cu}_{66}\text{Zn}_{34}$	0.08	0.2	0.5	52.5	3.8
$\text{Cu}_{47}\text{Zn}_{53}$				105	
$\text{Cu}_{43}\text{Zn}_{57}$				157.5	
$\text{Cu}_{17}\text{Zn}_{83}$				210	

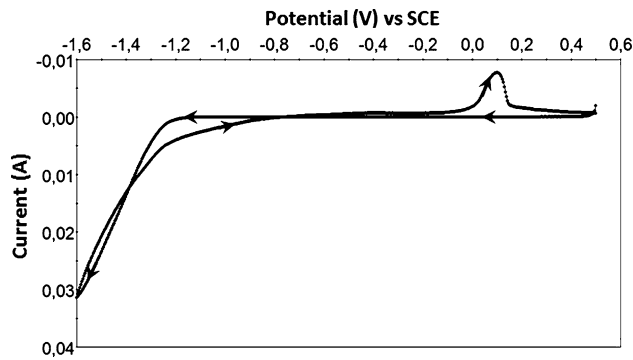
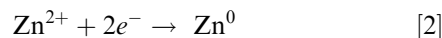
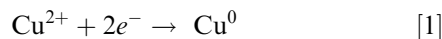


Fig. 1—Cyclic voltammograms for the system: aluminum substrate 0.2 (ZnSO₄·7H₂O), 0.08 (CuSO₄·5H₂O), 0.5 mol L⁻¹ (Na₃C₆H₅O₇), pH 5.8, temperature 293.15 K (20 °C), and scan rate 10 mV sn⁻¹.

applied potential value reaches -1.15 V. For higher potential values than -1.15 V, the cathodic current begins to increase and forms the cathodic peak at a potential that depends on the condition of the electrolyte.^[36] At this potential, both copper and zinc are co-discharged, and the alloy compositions consist of the partial currents of copper and zinc.

The cathodic reactions are:



The sharp increase in the current density at the potential values more negative than -1.5 V can be associated with a hydrogen evolution. On the reversal sweep, the cathodic current decreases slowly toward zero; after that, the anodic current starts to increase. Increase of the potential value in the more positive direction results in formation of an anodic peak as a consequence of the reaction.^[37] After that, metallic copper finishes its oxidative dissolution and current density decreases reaching a plateau at zero. In the anodic direction, a potential value is reached close to the equilibrium potential of the Cu/Cu²⁺. When the potential sweep is reversed, a hysteresis appears. Probably this crossover is related to the nucleation construction on the substrate.

B. The Effect of Applied Current on Electrodeposition of the Alloys

For co-deposition of the Cu-Zn alloys, diffusion plays a dominant role at the electrodeposition of the Cu and activation is the main factor for electrodeposition of the Zn.^[38] Increase in the current density results in an increase in cathodic overpotential and electron reaction velocity in the electrolyte. Generally, an increase in the reaction velocity results in an increase in the zinc content and in a decrease in the Cu content in the film. According to Brenner, increasing of the less noble metal (zinc) deposition mechanism can be explained with an increase in the current density.^[6] Probably an increase in the current density results in more negative cathode potential, which makes electrodeposition more easy.

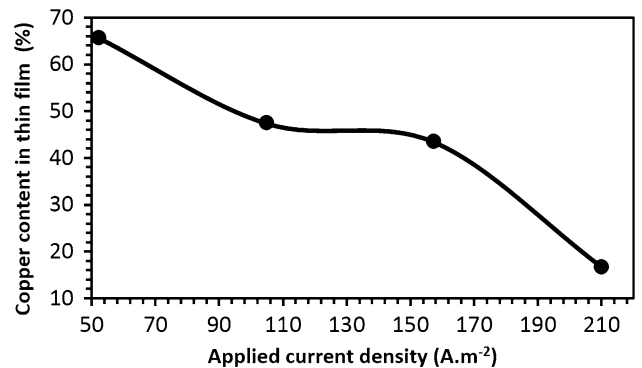


Fig. 2—EDX analysis results of the thin films deposited at varying current densities.

With increasing of the current density, the less noble metal (zinc) begins to deposit more preferentially. The relationship between copper content in the deposited alloy and the cathodic current density is indicated in Figure 2. It can be seen that a significant decrease in the copper content is observed with the increase of the current density. The Cu content in the Cu-Zn alloy changed in a range of 65.55 to 16.62 pct for higher current densities, despite the fact that the amount of Cu²⁺ ion concentration in the bath composition remains the same.^[38] This electrodeposition process is described as a regular alloy plating process.

The thin film compositions were designated by means of an energy-dispersive X-ray spectrometer (EDX). The EDX measurements were applied to the five different points of the films, and an average of these values was calculated. EDX analysis results of the deposited thin films were shown in Table II.

The various fabrication conditions performed in this study resulted in formation of alloys including different Zn and Cu amounts at different current densities. Probably an increase in the current density favored the formation of Zn nuclei, and thus, further growth of Cu particles was prevented.

C. XRD Analyses

The crystalline structure of the electrodeposited Cu-Zn films was analyzed by XRD experiments. The dominant peaks were used for all calculations. Figure 3 shows the XRD analysis results of the Cu_{1-x}Zn_x thin films deposited at varying current densities. The crystal orientation of an electrodeposit film is based on the deposition parameters,^[39,40] such as temperature, bath composition, current density, rinsing bath, and pH. Cu-Zn alloys including a high rate of zinc content comprises the α , β , and γ phases.^[16] Most peaks are sharp and well defined, indicating that coatings with a crystalline structure were obtained. From the XRD measurements of the alloys, alpha (α), beta (β), and gamma (γ) structure phases were detected. Both the α and γ phases were detected together for films deposited at current densities of 52.5, 105, and 210 A m⁻². Phases α , β , and γ were obtained from films deposited at the current density of 210 A m⁻².

Table II. EDX Analysis Results According to Applied Current Density Values

Thin Films	Current Density (A m ⁻²)	Electrolyte Composition		Film Composition	
		Cu (Pct)	Zn (Pct)	Cu (Pct)	Zn (Pct)
Cu ₆₆ Zn ₃₄	52.5	28.57	71.43	65.55	34.45
Cu ₄₇ Zn ₅₃	105			47.31	52.69
Cu ₄₃ Zn ₅₇	157.5			43.33	56.67
Cu ₁₇ Zn ₈₃	210			16.62	83.38

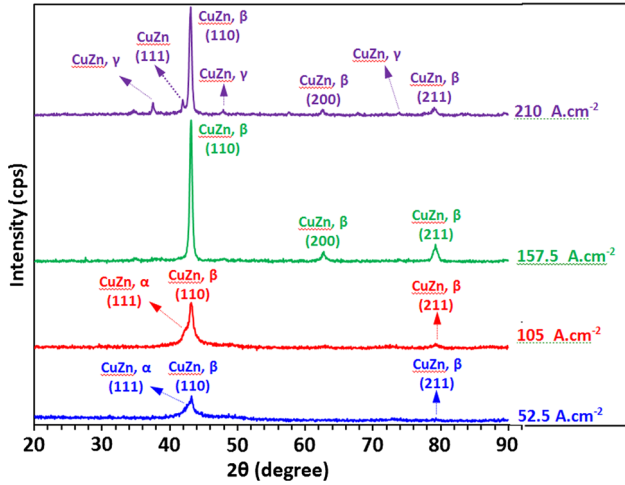


Fig. 3—XRD analysis results of the Cu_{1-x}Zn_x thin films deposited at varying current densities.

It is found that the intensities of (110) and (211) peaks are much higher than the other peaks, which indicates that these peaks are preferential crystal planes of the coatings. As seen in Figure 3, an increase of the current density toward 157.5 A m⁻² caused a great increase in the peak intensities of (110) and (211). But this behavior reversed for further increase of the current density. Relatively high current densities (210 A m⁻²) caused a decrease in the peak intensities of (110) and (211).^[16,32] XRD analyses results exhibited that the crystalline quality of the films first was increased suddenly with an increase in current density and then further decreased slightly after a critical point of the current.

XRD analysis peaks of the deposited alloys suggested the Cu-Zn alloys are in body-centered cubic (bcc) form and β phases. This result is in accordance with a previous study by Chen *et al.*^[40] The X-ray diffraction patterns of the Cu-Zn deposits exhibit a preferred orientation along the (111), (110), (200), (211), and (220) planes. With increase in the applied current density, the amount of copper in the alloy is reduced while the amount of the zinc is increased. Depending on the amount of applied current density, the phase structure of the film is shifted from α to γ. This change in the sample is caused by the change in the ratio of copper and zinc.

Calculated lattice parameters, average grain size, microstrain, and X-ray density *x* values as a function

of Cu and Zn concentration of the thin films are given in Table III. The grain size of the deposited thin films was calculated by Scherrer's formula (Eq. [3]) by using the peak width at the half maximum (β):

$$D = \frac{0.9\lambda}{\beta \cos \theta} \quad [3]$$

where *D* is grain size, β is full width at half maximum, λ is wavelength of X-ray, and θ is the diffraction angle.^[41,42]

Determining the exact effect of the current density on the grain size of the deposits is a complex problem due to the complexity of the electrodeposition mechanism. The charge transfer, electrochemical reactions, and cluster growth mechanisms are the main factors in electrodeposition. The effects of the current density are to a great extent complementary; by agitating the electrolyte, higher current values can be used before coarse coatings are formed. The average crystallite size of the Cu-Zn alloys increased and microstrain decreased with the increase of current densities.^[43] As shown in Figures 4 and 5, the lattice parameters decreased from 0.285 to 0.254 nm with an increase in the Zn content of the film from 34 to 83 pct for the Cu-Zn alloys. The microstrain of thin films were calculated by using the following relations:^[44]

$$\varepsilon = \frac{\beta \cdot \cos \theta}{4} \quad [4]$$

The microstrains (ε) for preferential orientation were calculated using Eq. [4]. The microstrains were found to be within the range of approximately 0.111 to 0.171 as seen in Figure 6.

The X-ray densities of the alloys were obtained using Eq. [5]:^[45]

$$\rho = \frac{2M}{N_a a^3} \quad [5]$$

where *M* is the molecular weight of the alloys, *N_a* is Avogadro's number, *a* is the lattice parameter, and 2 is the number of molecules in the unit cell. According to the calculations, the X-ray density increased from 9.21 to 13.19 g/cm³ with an increase in the applied current density. It is suggested that X-ray density is contingent on the lattice parameters. As shown in Table III, a decrease in the lattice parameters was observed after an increase of the Zn content accompanied by an increase in the corresponding X-ray density.

Table III. Calculated Grain Size, Microstrain, Lattice Parameter, and X-ray Density of the ZnCu Alloys from XRD Measurements

Alloys	2θ (Degrees)	d (Å)	Intensity (Cps)	FWHM	Microstrain (ϵ)	Grainsize (D) (nm)	Lattice (a) (nm)	X-ray Density ρ (g/cm ³)
Cu ₆₆ Zn ₃₄	43.200	2.0925	188	0.501	0.155	76	0.285	9.21
Cu ₄₇ Zn ₅₃	43.149	2.0948	402	0.582	0.171	66	0.269	11.01
Cu ₄₃ Zn ₅₇	43.147	2.0949	1729	0.429	0.126	89	0.268	11.15
Cu ₁₇ Zn ₈₃	43.096	2.0973	1280	0.402	0.111	95	0.254	13.19

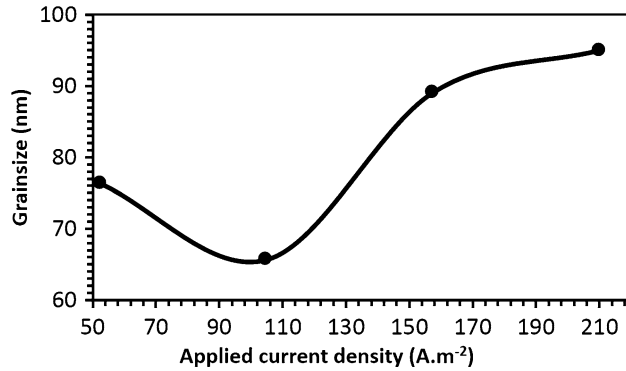


Fig. 4—Effect of applied current density on the grain size.

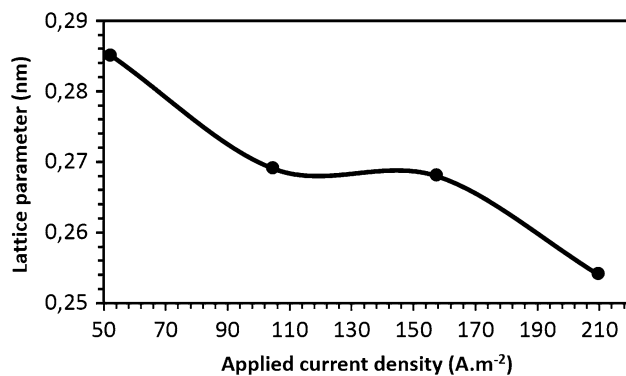


Fig. 5—Effect of applied current density on the lattice parameter.

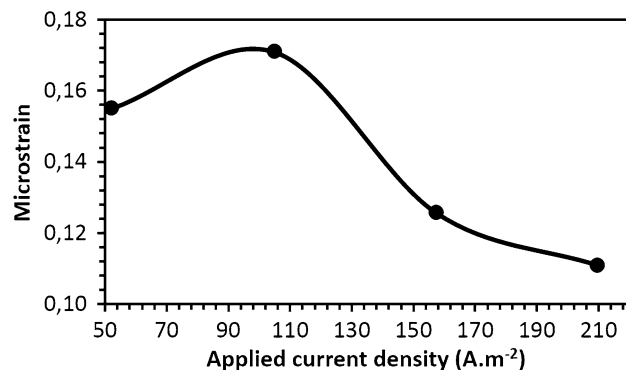


Fig. 6—Effect of applied current density on the microstrain.

As expected, both microstrain and dislocation density behaviors of the films are in reverse manner with the grain size. According to XRD patterns, a shift in peak

positions was observed toward values lower than 2, with increasing of the current density. This shift indicates a decrease in the lattice strains of the structures.

D. The Effect of Current on the Morphology of the Coated Alloys

Figure 7 displays the surface morphology of the alloys deposited at different current densities of 52.5, 105, 157.5, and 210 A m⁻². According to the morphology studies, it is observed that the grain structure of the electrodeposited Cu-Zn coatings is influenced by applied current density.

There is a strict correlation between current densities and formation of the coating. An increase in the current density affects the grain formation from small to bigger grained crystallites as a result of deposition rates. A considerable change in the shape of the crystallites was also observed with the higher current densities. As the applied current density increased from 52.5 to 210 A m⁻², the grain size of the electrodeposited Cu-Zn was also increased. For coatings deposited at 105 and 157.5 A m⁻², the apparent grain size is increased slightly compared with the alloys deposited at 52.5 and 105 A m⁻². As the current density increases up to 157.5 A m⁻², larger grains are observed on the surface of the coating. The increased grain size might be a result of hydrogen evolution, which was observed at the surface of the coating during depositing with current density values of higher than 105 A m⁻². Increasing of hydrogen evolution levels may hinder the adsorption of the plating additives onto the film during deposition results to increased grain size. Hydrogen evolution may also increase mass transport and improve grain growth rather than fresh nucleation.^[46] Some studies showed that fine-grained, smooth, and compact deposits of the alloys are obtained by the addition of sodium citrate.^[47] Ferreira *et al.* observed that shiny coatings whose colors vary from red to yellow-reddish electrodeposits were obtained at equal or higher than 0.5 mol L⁻¹ containing citrate bath sodium citrate concentrations.^[21]

E. Electrical Resistivity Measurements

The electrical resistivity values of the thin films deposited with the various current densities were calculated with a four-point measurement method. The electrical resistivity measurements were performed in a temperature range of 100 K to 350 K (−173 °C to 77 °C). Measured resistivity values of the films were graphed as a function of temperature in Figure 8. The

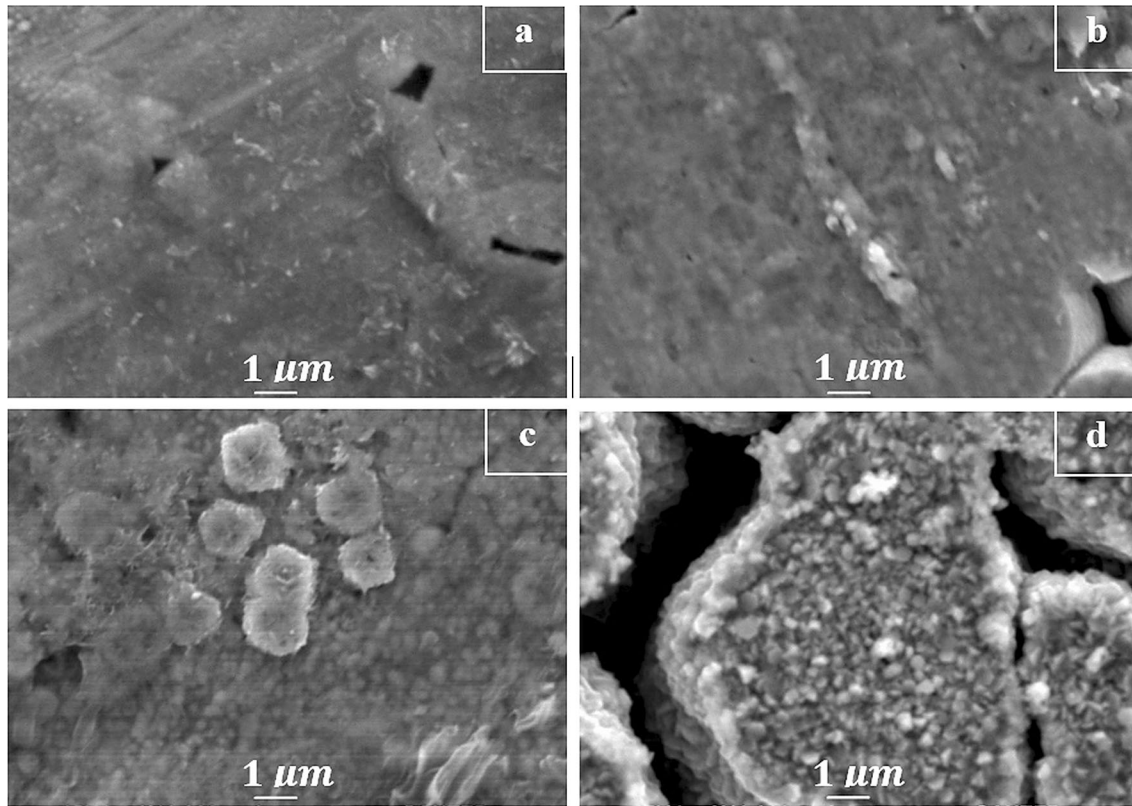


Fig. 7—SEM images of the (a) $\text{Cu}_{66}\text{Zn}_{34}$ alloy, (b) $\text{Cu}_{47}\text{Zn}_{53}$ alloy, (c) $\text{Cu}_{43}\text{Zn}_{57}$ alloy, and (d) $\text{Cu}_{17}\text{Zn}_{83}$ alloy.

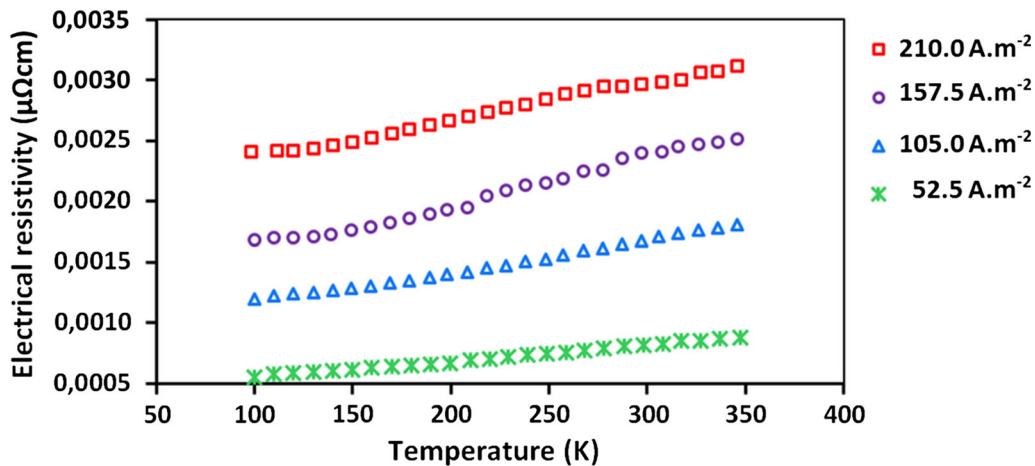


Fig. 8—Effect of the temperature on the electrical resistivity of the alloys deposited at various current densities.

figure displayed the effect of applied current density on the electrical resistivity at various temperatures. This technique can make microstructural characterization and detect different microstructural features of the alloys by analyzing resistivity. According to analysis results, the highest resistivity was observed for the $\text{Cu}_{17}\text{Zn}_{83}$ alloy (deposited at 210 A m^{-2}) and the smallest one was detected for the $\text{Cu}_{47}\text{Zn}_{53}$ alloy (deposited at 105 A m^{-2}). There is a significant increase in the resistivity values above a critical temperature

value of 100 K ($-173 \text{ }^\circ\text{C}$). This behavior can be assigned to the phonon scattering of the conduction electrons.^[48] The increased resistivity with the current density is probably a result of increasing disorder, caused by a higher Zn amount in the alloy,^[49] which contributes to the increasing electron scattering results increasing resistivity.^[50] The resistance of the films decreased with the decrease of temperature, suggesting that the electrical transport mechanism is metallic. In metals, one can usually identify several scattering mechanisms at the low

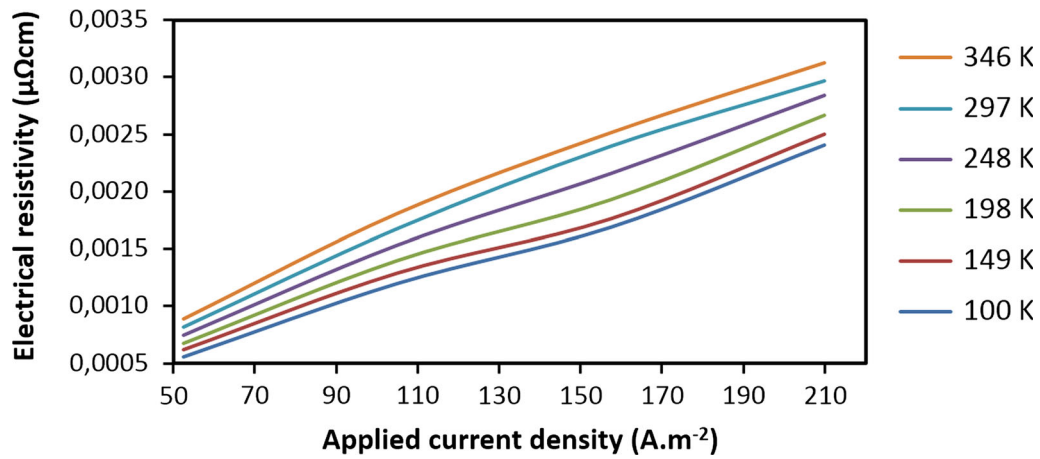


Fig. 9—Effect of the current density on the electrical resistivity at various temperatures.

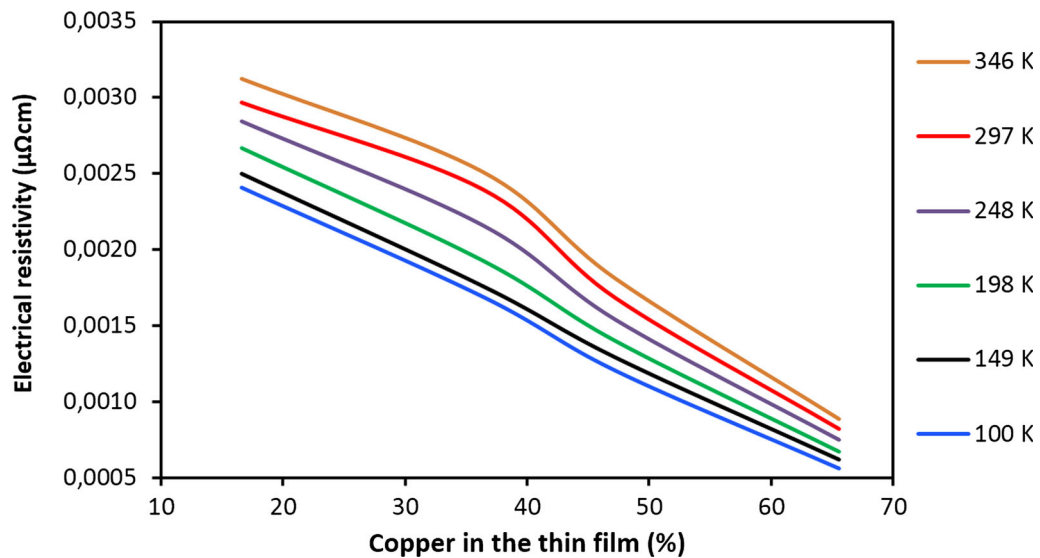


Fig. 10—Effect of the Cu content on the electrical resistivity at various temperatures.

temperatures: phonons, magnons, and electron–electron scattering, each giving rise to different power-law temperature dependences.^[51]

All deposited films exhibited a positive temperature-coefficient (PTC) resistivity. This indicates an important role of lattice vibrations for the temperature dependence of electrical resistivity.^[48–52] The most interesting behavior of PTC materials is their higher electrical resistivity at higher temperatures. The PTC effect is related to the grain boundary effect. As a consequence of lower grain size values, an increase in the number of grain boundaries and a decrease in the average voltage across the single-grain boundary will be observed. Hence, the total value of the breakdown voltage increases.^[53] Obtained residual resistivity values of the films are 0.00056, 0.0012, 0.0017, and 0.0024 $\mu\Omega$ cm for the $\text{Cu}_{66}\text{Zn}_{34}$ (52.5 A m^{-2}), $\text{Cu}_{47}\text{Zn}_{53}$ (105 A m^{-2}), $\text{Cu}_{43}\text{Zn}_{57}$ (157.5 A m^{-2}), and $\text{Cu}_{17}\text{Zn}_{83}$ (210 A m^{-2}) alloys, respectively. Decrease of the copper in the

film from the 66 pct to 17 pct caused an increase in the obtained residual resistivity. The total increase in the resistivity from 100 K to 350 K (–173 °C to 77 °C) was calculated by the following equation:

$$R = (\rho_{350\text{K}} + \rho_{100\text{K}}) / \rho_{100\text{K}} \quad [6]$$

Calculated values are 58.3, 50.4, 48.6, and 29.7 pct for the films deposited at a current density of 52.5, 105, 157.5, and 210 A m^{-2} , respectively. Copper exhibits slightly higher values than the zinc, which may be attributed to the grain boundaries in the sample that act as an additional scattering center. Taslimi *et al.* obtained similar results for metallic CoFe alloys.^[54]

Figure 9 shows the effect of applied current density vs analysis temperature on the electrical resistivity. The electrical resistivity vs Cu amount in the alloy is displayed in Figure 10. The resistivity increased with the increase of applied current densities.^[55] Figure 9

indicated a strong relationship between the resistivity and composition of the films. The electrical resistivity values increased with Cu concentrations in the films. This strong dependence on the composition can be related to the densities of states.

IV. CONCLUSIONS

The effect of the applied current density on the physical and the structural properties of the Cu-Zn films deposited was investigated. The results of the study revealed that the applied current density in electrodeposition affects the phase structure, grain size, microstrain, and electrical resistivity of the deposited Cu-Zn alloys. According to XRD analysis results, deposited Cu-Zn films have a crystalline structure with the presence of bcc ($\alpha + \beta$), β , and ($\beta + \gamma$) phases. A change in the crystalline structure of the film was observed with a change in the applied current density. While the intensity of the main Cu-Zn β (111) peak increased with an increase of the current density from 52.5 to 105 A m⁻², the intensity of the bcc Cu-Zn γ (110) peak decreased. The crystallite size of the films decreased with the increasing applied current density. The most interesting result was the increase of the Zn content in the deposited alloys with an increase of the applied current density according to compositional analysis. SEM analysis indicated the surface morphology of Cu-Zn films is also affected from the applied current density. According to the four-probe measurements, the electrical resistivity of the films increased with an increase of the current density, which probably resulted in an increase of the disorder due to higher Zn content of the alloy. Results of this study indicate that properties of the alloy films can be controlled by controlling the electrodeposition parameters. Further studies can lead to fabricate alloys with desired properties with a controlled electrodeposition method.

ACKNOWLEDGMENTS

Financial support of this research by the Mustafa Kemal University Scientific Research Projects is gratefully acknowledged (MKU-BAP- 1005 M 0118 and 1204 D 0110).

REFERENCES

- J. Chen, C. Ruffert, H.H. Gatzert, R. Bandorf, and G. Bräuer: *Design and Manufacturing of Active Microsystems Microtechnology and MEMS*, Springer, Berlin, 2011, pp. 167–88.
- M. Paunovic and M. Schlesinger: *Fundamentals of Electrochemical Deposition*, Wiley, 2006.
- F.A. Lowenheim: *Electroplating*, McGraw-Hill, Columbus, OH, 1978, p. 378.
- I.A. Carlos and M.R.H. de Almeida: *J. Electroanal. Chem.*, 2004, vol. 562, pp. 153–59.
- T. Vagramyan, J.S.L. Leach, and J.R. Moon: *Electrochim. Acta*, 1979, vol. 24, pp. 231–36.
- A. Brenner: *Electrodeposition of Alloys*, Academic Press, New York, 1963, vol. 1, p. 411.
- E.M. Oliveira, G.A. Finazzi, and I.A. Carlos: *Surf. Coat. Technol.*, 2006, vol. 200, pp. 5978–85.
- Y. Fujiwara and H. Enomoto: *Surf. Coat. Technol.*, 1988, vol. 35, no. 1,2, pp. 101–11.
- K. Johannsen: *Surf. Finish.*, 2001, vol. 88, pp. 104–08.
- L.F. Senna, S.L. Díaz, and L. Sathler: *J. Appl. Electrochem.*, 2003, vol. 33, pp. 1155–61.
- F.L.G. Silva, D.C.B. do Lago, and L.F. Senna: *J. Appl. Electrochem.*, 2010, vol. 40, pp. 2013–22.
- I.G. Casella: *J. Electroanal. Chem.*, 2002, vol. 520, nos. 1,2, pp. 119–25.
- D. Defilippo, A. Rossi, and D. Atzei: *J. Appl. Electrochem.*, 1992, vol. 22, pp. 64–72.
- P. De Vreese, A. Skoczylas, E. Matthijs, J. Fransaeer, and K. Binnemans: *Electrochim. Acta*, 2013, vol. 108, pp. 788–94.
- V.V. Povetkin, M.S. Zakharov, and R.R. Muslimov: *Russ. J. Appl. Chem.*, 1999, vol. 72 (8), pp. 1367–69.
- R. Juskenas, V. Karpavičienė, V. Pakštas, A. Selskis, and V. Kapočius: *J. Electroanal. Chem.*, 2007, vol. 602, pp. 237–44.
- J.C. Ballesteros, L.M. Torres-Martínez, I. Juárez-Ramírez, G. Trejo, and Y. Meas: *J. Electroanal. Chem.*, 2014, vol. 727, pp. 104–12.
- J.C. Ballesteros, C. Gomez-Solis, L.M. Torres-Martínez, and I. Juárez-Ramírez: *Int. J. Electrochem. Sci.*, 2015, vol. 10, pp. 2892–903.
- A. Survila, Z. Mockus, S. Kanapeckaitė, G. Stalnionis, R. Juskenas, and V. Jasulaitiene: *J. Electrochem. Soc.*, 2013, vol. 160, pp. D428–33.
- L. Mattarozzi, S. Cattarin, N. Comisso, R. Gerbasi, P. Guerriero, M. Musiani, L. Vazquez-Gomez, and E. Verlato: *J. Electrochem. Soc.*, 2015, vol. 162 (6), pp. D236–41.
- F.B.A. Ferreira, F.L.G. Silva, A.S. Luna, D.C.B. Lago, and L.F. Senna: *J. Appl. Electrochem.*, 2007, vol. 37, pp. 473–81.
- R. Özdemir and I.H. Karahan: *Appl. Surf. Sci.*, 2014, vol. 318, pp. 314–18.
- I.H. Karahan and R. Özdemir: *Appl. Surf. Sci.*, 2014, vol. 318, pp. 100–04.
- F.H. Assaf, S.S.A. Elrehim, A.S. Mohamed, and A.M. Zaky: *Indian J. Chem. Technol.*, 1995, vol. 2, pp. 147–52.
- E. Chaissang, K.V. Quang, and R. Wiart: *J. Appl. Electrochem.*, 1986, vol. 16, pp. 591–604.
- V.N. Gusev, A.L. Bezzubov, and E.D. Kochman: *Sov. Electrochem.*, 1977, vol. 13 (1), p. 111.
- F.B.A. Ferreira, P.K.C. Afonso, A.S. Luna et al.: *Proceedings of the 2nd Mercosur Congress on Chemical Engineering*, Rio de Janeiro, 2005.
- I.H. Karahan, R. Ozdemir, and B. Erkeyman: *Appl. Phys. A*, 2013, vol. 113, pp. 459–76.
- N.C. Kotsakis, P. Raptopoulou, V. Tangoulis, A. Terzis, J. Giapintzakis, T. Jakusch, T. Kiss, and A. Salifoglou: *Inorg. Chem.*, 2003, vol. 42 (1), pp. 22–31.
- M.R.H. de Almeida, E.P. Barbano, M.F. de Carvalho, I.A. Carlos, J.L.P. Siqueira, and L.L. Barbosa: *Surf. Coat. Technol.*, 2011, vol. 206, pp. 95–102.
- E.G. Vinokurov, K.L. Kandyrin, and V.V. Bondar: *Zhurnal Prikladnoi Khimii*, 2010, vol. 83 (4), pp. 606–10.
- J. Stevanovic, L.J. Skibina, M. Stefanovic, A. Despic, and V.D. Jovic: *J. Appl. Electrochem.*, 1992, vol. 22, pp. 172–78.
- C. Rousse, S. Beaufils, and P. Fricoteaux: *Electrochim. Acta*, 2013, vol. 107, pp. 624–31.
- S.S. Kulkarni and C.D. Lokhande: *Mater. Chem. Phys.*, 2003, vol. 82 (1), pp. 151–56.
- K.G. Suresh and K.V.S. Rama Rao: *J. Alloys Compd.*, 1996, vol. 238, no. 1,2, pp. 90–94.
- D. Grujicic and B. Pesic: *Electrochim. Acta*, 2002, vol. 47 (18), pp. 2901–12.
- R. Berry, P. Hall, and M. Harris: *Thin Film Tech*, Van Nostrand Reinhold Co., Florence, 1968.
- Y. Li, H. Jiang, W. Huang, and H. Tian: *Appl. Surf. Sci.*, 2008, vol. 254 (21), pp. 6865–69.
- I.H. Karahan: *J. Mater. Sci.*, 2007, vol. 42 (24), pp. 10160–63.
- P.Y. Chen, M.Y. Lin, and I.W. Sun: *J. Electrochem. Soc.*, 2000, vol. 147, no. 9, pp. 3350–55.

41. M. George, S.S. Nair, A.M. John, P.A. Joy, and M.R. Anantharaman: *J. Phys. D*, 2006, vol. 39, pp. 900–10.
42. S. Nasir, M. Anis-ur-Rehman, and M.A. Malik: *Phys. Scripta*, 2011, vol. 83, p. 25602.
43. M.A. Kumar and S. Muthukumaran: *J Mater Sci*, 2013, vol. 24, pp. 4050–59.
44. K.L. Chopra: *Thin Film Phenomena*, McGraw-Hill, Columbus, OH, 1969.
45. J. Smit and H.P.J. Wijn: *Ferrites*, Wiley, New York, 1959.
46. M.A. Ashworth, G.D. Wilcox, R.L. Higginson, R.J. Heath, C. Liu, and R.J. Mortimer: *Microelectron. Reliab.*, 2015, vol. 55, pp. 180–91.
47. A. Afshar, A.G. Dolati, and M. Ghorbani: *Mater. Chem. Phys.*, 2003, vol. 77 (2), pp. 352–58.
48. J. Dolinsek, T. Apih, P. Jeglic, I. Smiljanic, A. Bilušić, Ž. Bihar, A. Smontara, Z. Jagličić, M. Heggen, and M. Feuerbacher: *Intermetallics*, 2007, vol. 15, pp. 1367–76.
49. D.C. Leitao, C.T. Sousa, J. Ventura, J.S. Amaral, F. Carpinteiro, K.R. Pirota, M. Vazquez, J.B. Sousa, and J.P. Araujo: *J. Non-Cryst. Solids*, 2008, vol. 354, pp. 5241–43.
50. V. Chaudhari, S.E. Shirsath, M.L. Mane, R.H. Kadam, S.B. Shelke, and D.R. Mane: *J. Alloy. Compd.*, 2013, vol. 549, pp. 213–20.
51. A. Gerber, A. Milner, I.Y. Korenblit, M. Karpovsky, A. Gladkikh, and A. Sulpice: *Phys. Rev. B*, 1998, vol. 57, p. 13667.
52. I.H. Karahan, O. Karabulut, and U. Alver: *Phys. Scripta*, 2009, vol. 79, p. 055801V.
53. D.H. Kim, I.K. Park, W.S. Um, and H.G. Kim: *Jpn. J. Appl. Phys.*, 1995, vol. 34, pp. 4862–69.
54. H. Taslimi, M.H. Sohi, S. Mehrizi, and M. Saremi: *J. Mater. Sci.*, 2015, vol. 26, pp. 2962–68.
55. C.M. Lee, S.M. Hwanga, G.C. Parka, J.C. Kima, J.H. Lima, J. Joo, S.-B. Junga, and Y.S. Kim: *Curr. Appl. Phys.*, 2011, vol. 11 (4), pp. S128–31.